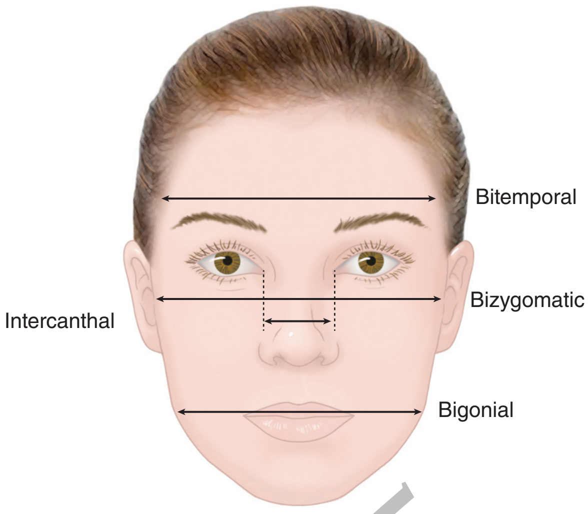

Fig. 1.3 The widest portion of the face is bizygomatic distance with the bitemporal and bigonial distances being approximately equal to and 10% less than the widest portion of the face. The intercanthal distance approximates the distance between the alar lobules.)

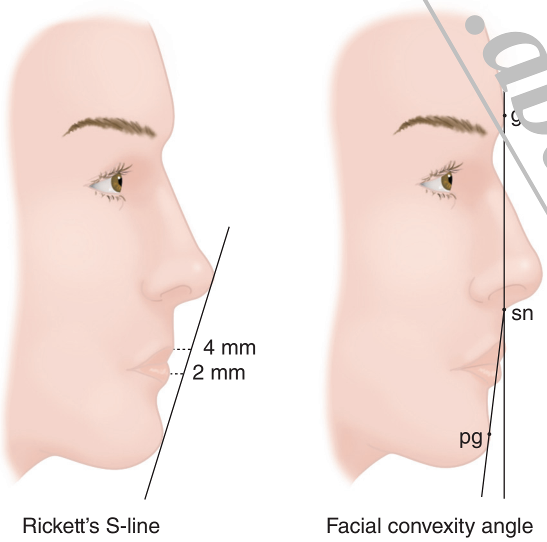

Fig. 1.4 The position of the chin point can be assessed by several methods. Using Rickett's method, a line is drawn from nasal tip to chin point. The upper and lower lip should lie 4 mm and 2 mm posterior to this line, respectively. Greater or lesser amounts of these measurements will indicate a retrusive or prominent chin if the nasal and maxillary positions are normal. An alternative method is to draw a perpendicular line from the glabella through the subnasale in the head held in a horizontal plane. The chin point should lie within a few millimeters of such a line. (With permission from: Bartlett SP, Wornom I, 3rd, Whitaker LA. Evaluation of facial skeletal aesthetics and surgical planning. Clin Plast Surg 1991;18:1–9.)

definable soft tissue measurements based on the bony structure (see Chapter 44).[27] The highlight areas are the temporal ridge–supraorbital ridge structures, the malar–midface structures and the mandible–chin structures. The lowlight areas are those in between, above, and below. Thus the lowlight areas are the forehead sloping above the supraorbital ridge, the temporal concavities below the temporal ridges, the orbits and lateral orbital rims below the supraorbital ridges, the perioral–lateral soft tissue cheek areas below the malar midface structures and above the mandible, and the submandibular area. The lowlight areas can potentially be further deemphasized and the highlight areas increasingly highlighted.

In the forehead and temporal region, from the glabella, the forehead curves smoothly posteriorly[27] as one proceeds toward the trichion making an approximately –7 degrees in females and –10 degrees in males as shown in Fig. 1.5. A gentle curve is also seen from the glabella transversely to the malar region, with the most anterior projection occurring along the curve at the mid eyebrow region. The temporal crest interrupts the forehead into sagittal and transverse plates as it joins the superior lateral orbit to create the temporal hollow. In the profile view, the nasofrontal angle forms a distinct landmark, measuring about 130 to 135 degrees, appearing more acute in the male population.[27]

In the orbital region, the superior orbital rim is immediately subjacent to the eyebrow, as a visible promontory in the young harmonious face.[27] The intercanthal distance often approximates the inner to outer canthal distance in about a third of the population, whereas it is greater or lesser in the rest of the population.[28] In the harmonious male face, the outer canthus is 2.1 mm higher than the inner canthus, whereas in the female face, the distance is noted to be 4.1 mm; thus the eye fissure inclines upward moving from medial to lateral. Another significant feature viewed from the profile view is the relationship between the most anterior surface of the cornea and the position of the supraorbital ridge and lateral orbital rim. From the profile view, as shown in Fig. 1.6, the

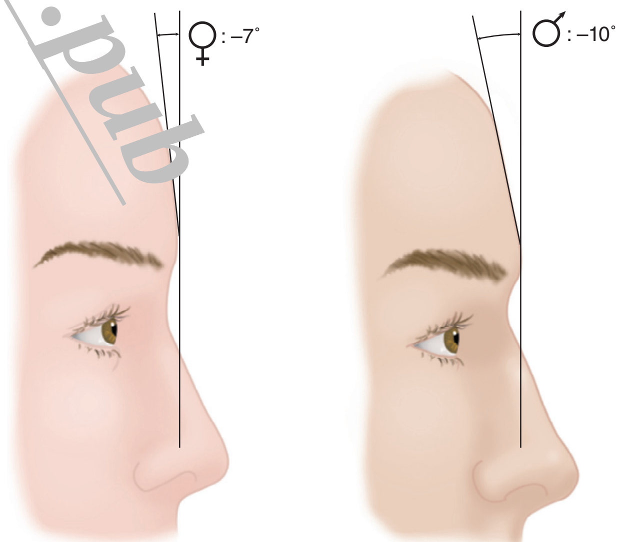

Fig. 1.5 The forehead inclination differs in the ideal face in male and the female with female face showing a steeper inclination while the nasofrontal angle is typically more acute in the male face. (With permission from: Bartlett SP, Wornom I, 3rd, Whitaker LA. Evaluation of facial skeletal aesthetics and surgical planning. Clin Plast Surg 1991;18:1–9.)

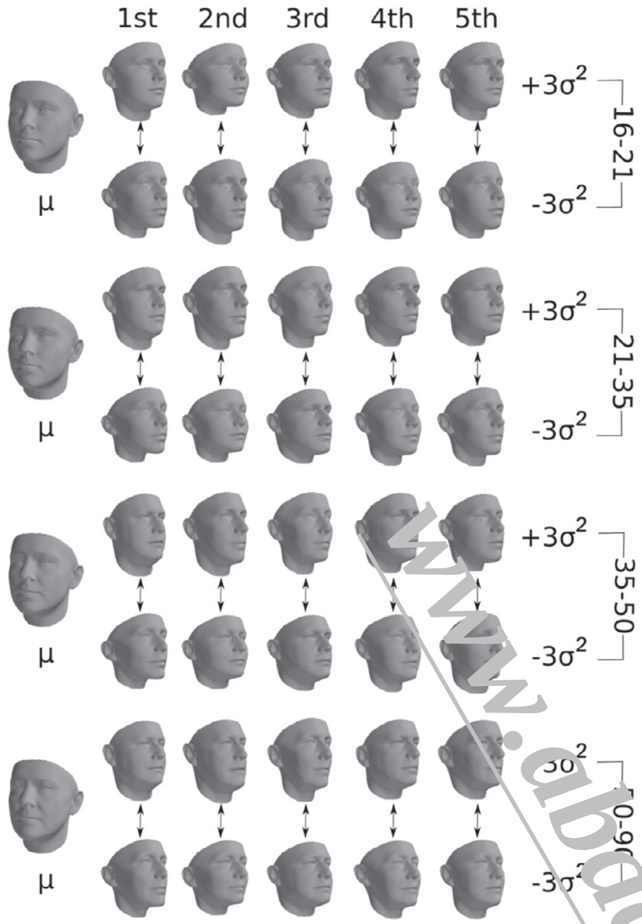

Fig. 3.6 Mean face and first five principal components per group years of age: 16 to 21, 21 to 35, 35 to 50, and 50 to 90 years.

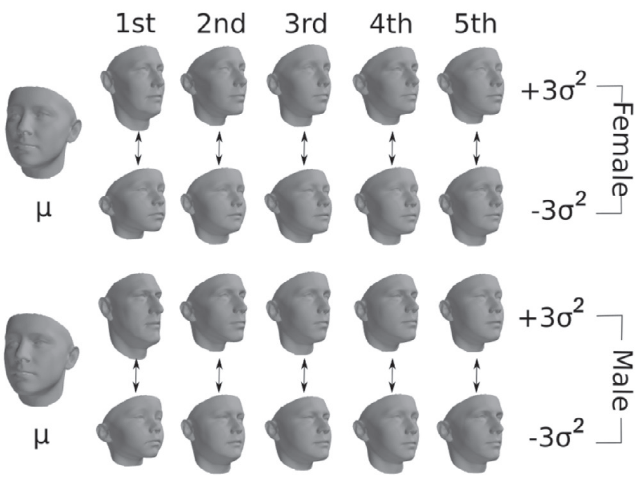

Fig. 3.7 Mean face and first five principal components of female and male populations.

population. The population is described by the mean face and its principal components of variation (eigenvectors) describing a multidimensional face space or face manifold. There are several thousand possible eigenvectors within a facial model, but nearly all of the variations within the model are described in the first 100 principal components. Individual faces can

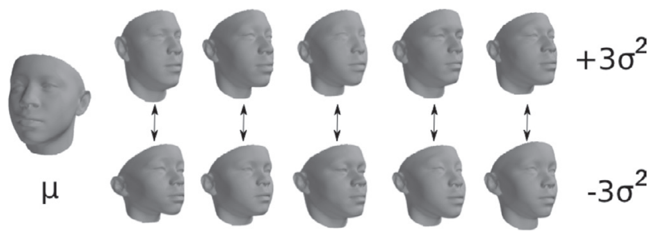

Fig. 3.8 Mean face and first five principal components of black population.

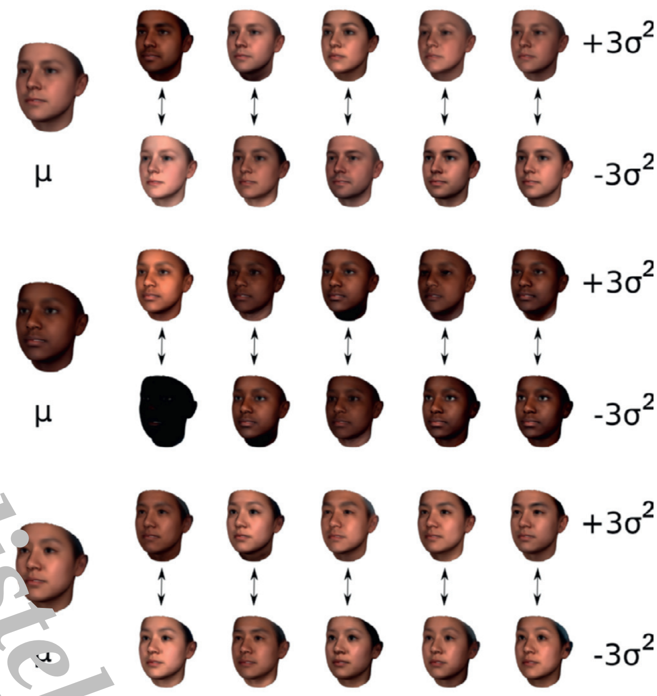

Fig. 3.9 Mean face with texture and first five principal components of white population (top); black population (middle); and Asian population (bottom).

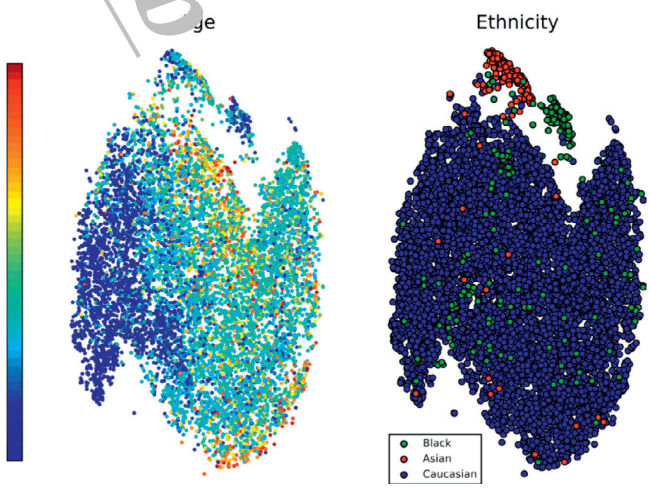

Fig. 3.10 T-distributed Stochastic Neighbor Embedding (t-SNE) plot: Identifying subgroups within a population.

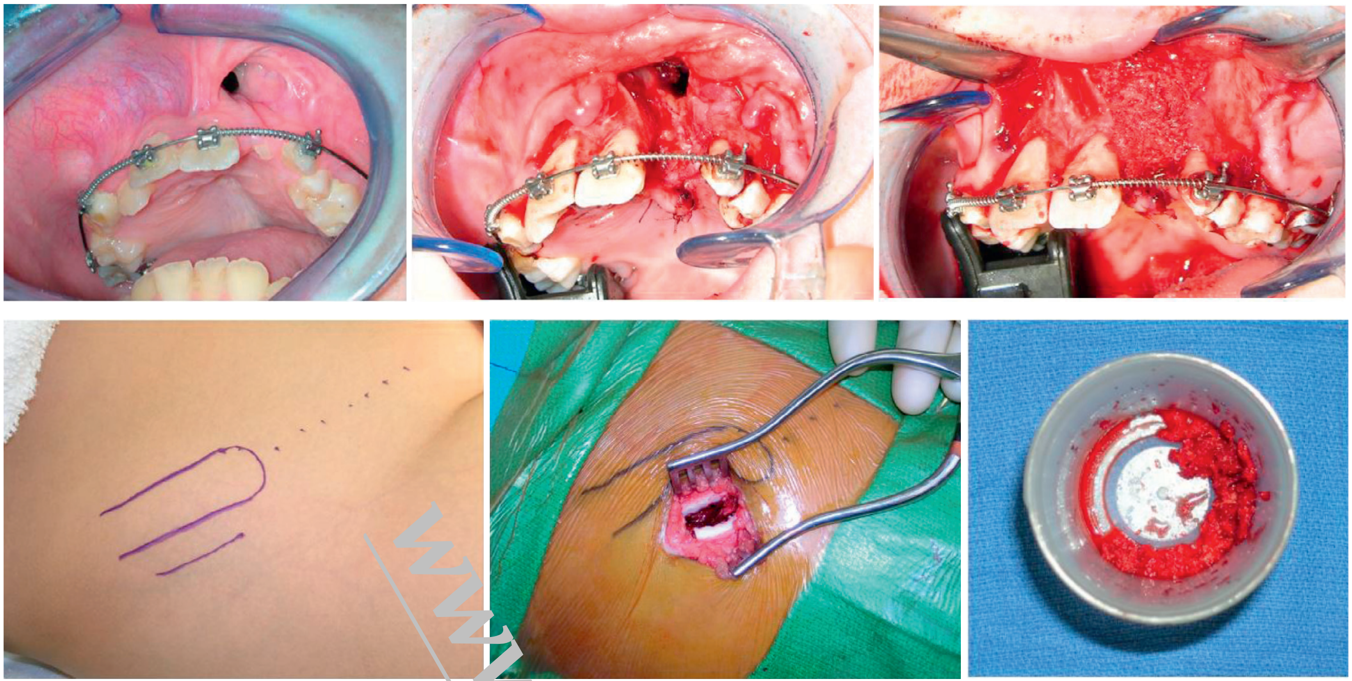

Fig. 11.3 Alveolar cleft repair using an iliac cancellous bone graft. This is a 10-year-old male with a left cleft lip and palate. Standard cleft lip and palate care includes grafting of the alveolar cleft before the eruption of the canine. The most common site for bone grafting is the iliac crest, where cancellous bone is retrieved under general anesthesia while the alveolar cleft is exposed. This graft has a large surface area, which leads to rapid remodeling and incorporation. The cleft is an example of an inlay bone graft and is not an immediate high load-bearing site. After the bone graft is consolidated, the patient will undergo eventual dental implant placement with load-bearing function. (Courtesy of Dr. Janice S. Lee, while at UCSF, Department of Oral & Maxillofacial Surgery.)

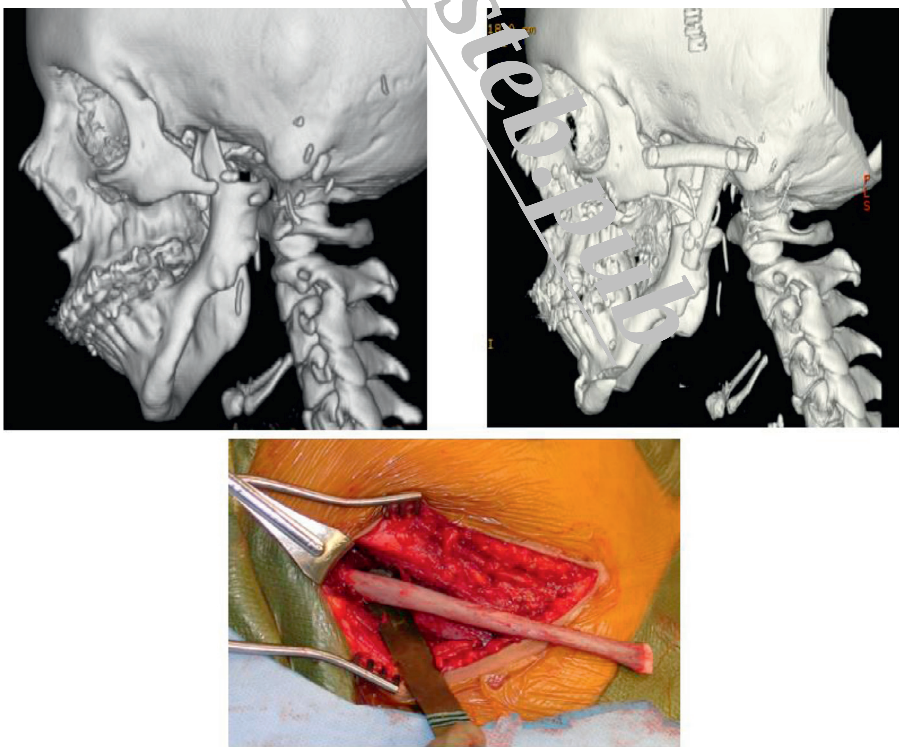

Fig. 11.4 Temporomandibular joint (TMJ) construction using a costochondral bone graft. This is a 16-year-old female with left dominant hemifacial microsomia. The missing left condyle, glenoid fossa, and zygomatic arch were constructed with a costochondral bone graft. The hyaline cartilage cap was maintained on the articulating surface of the graft to allow normal function as a joint, and the constructed glenoid fossa was lined with a temporoparietal fascial flap. (Courtesy of Dr. Janice S. Lee, while at UCSF, Department of Oral & Maxillofacial Surgery.)

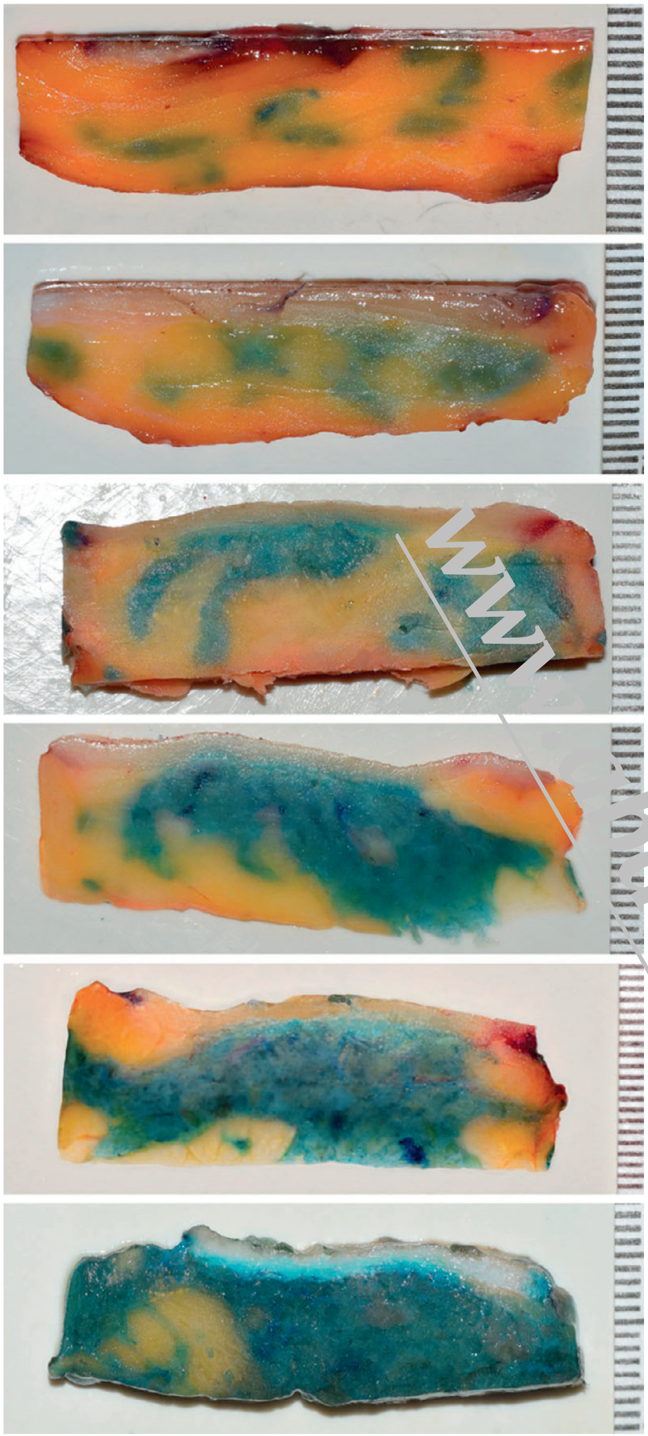

Fig. 14.3 Representative sections of pannus after injection of fat graft stained with methylene blue. First row, Fat grafted at a volume ratio of 1:10. Second row, Fat grafted at a volume ratio of 1:8. Third row, Fat grafted at a volume ratio of 1:6. Fourth row, Fat grafted at a volume ratio of 1:4. Fifth row, Fat grafted at a volume ratio of 1:2. Sixth row, Fat grafted at a volume ratio of 1:1. (Reproduced from Bourne DA, et al. The architecture of fat grafting: what lies beneath the surface. Plast Reconstr Surg 2016;137(3):1072–9, with permission).

The first additive to be discussed is ASCs, which have proven to increase angiogenic and wound-healing capacity. ASCs reside in the perivascular compartments of the stroma of adipose tissue. Adipose tissue needs to undergo enzymatic digestion with collagenase, followed by lysis of red blood cells to produce SVF, which contains various progenitor cells, such as ASCs, pericytes, transit amplifying cells, and endothelial progenitor cells. To isolate ASCs, SVF is plated on tissue culture plastic, where ASCs adhere preferentially. Other nonenzymatic approaches, including washing and mechanical separation, have been developed but are not as common. Whether it is supplementing lipoaspirate with SVF or ASCs or enriching these cells through centrifugation, all of these methods have enhanced fat graft retention and improved clinical outcomes by providing sites of adipogenesis in zones where the graft would otherwise not survive, as well as improving vascular support via endothelial cell proliferation.

Very strong preclinical and clinical evidence supports the benefit of ASC-enriched fat grafting. In a landmark clinical study, Yoshimura et al. introduced cell-assisted lipotransfer (CAL) or SVF-enriched fat grafting by reporting a very high graft retention in 40 patients undergoing CAL of breast augmentation.[41] Kølle et al. conducted a triple-blinded randomized controlled trial of 10 patients receiving ASC-enriched or nonenriched fat grafting and found improved retention, enhanced formation of new connective tissue, and reduced fat graft necrotic tissue in patients receiving ASC-enriched fat graft.[42] Tanikawa et al. conducted a randomized controlled trial in 14 patients with craniofacial microsomia treated with either ASC-enriched or nonenriched fat grafting and found significant improvement in volume retention at 6 months.[43] Similar results were obtained by Koh et al., who conducted a randomized controlled trial in 10 patients with hemifacial atrophy secondary to Parry-Romberg disease, again treated with either ASC-enriched or nonenriched microfat grafting; patients treated with enriched graft had improved graft survival.[44] These are some of the many studies that examined the role of ASCs as an additive in fat grafting and certainly make a strong case of their clinical benefit. However, longer-term studies looking at safety and graft retention are needed before clinical adoption by the whole surgical community.

Platelet-rich plasma (PRP) is another additive that, in recent years, has become more frequently used because of its regenerative properties. PRP is obtained by centrifuging whole blood to obtain a five to seven times concentration of platelets (minimum standard for PRP of 106 platelets/mL) suspended in a small volume of plasma, which is then activated by using bovine thrombin and calcium chloride to trigger degranulation of granules. The activated platelets release various growth factors, including platelet-derived growth factor, vascular endothelial growth factor (VEGF), transforming growth factor-β_1 and β_2, epidermal growth factor, and thrombospondin. Thus far, the use of PRP as an additive in fat grafting has shown great promise in vitro. Our laboratory showed that PRP significantly enhances ASC proliferation, even in the presence of antiproliferative, proadipogenic media. However, PRP inhibits adipogenic differentiation demonstrated by decreased intracellular

Fig. 18.5 Patient with facial skeletal asymmetry illustrating the use of the SureSmile process for combined orthodontic and orthognathic surgery.

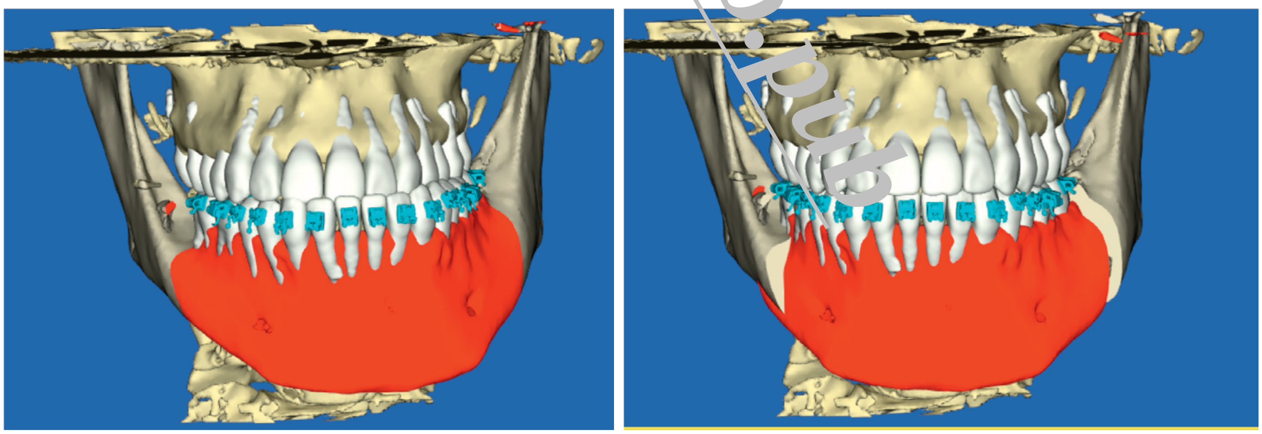

Fig. 18.6 Virtual planning of dental movement with skeletal movement.

the wire sizes were slightly smaller. Fig. 18.7 shows an example of the upper and lower arch wire design. Each set of wires is allowed to express for 8 weeks, and most cases are adequately aligned after the first two sets of wires. However, one of the benefits of SureSmile over some of the other CAD/CAM systems is that it enables the orthodontist to easily create adjustments in the software wire design on the basis of clinical chairside observations. Additional "modification" wires are provided at no additional cost.

In the previously mentioned case, 6 weeks before the procedure, new presurgical records were taken. These included a full set of photos (Fig. 18.8), CBCT in

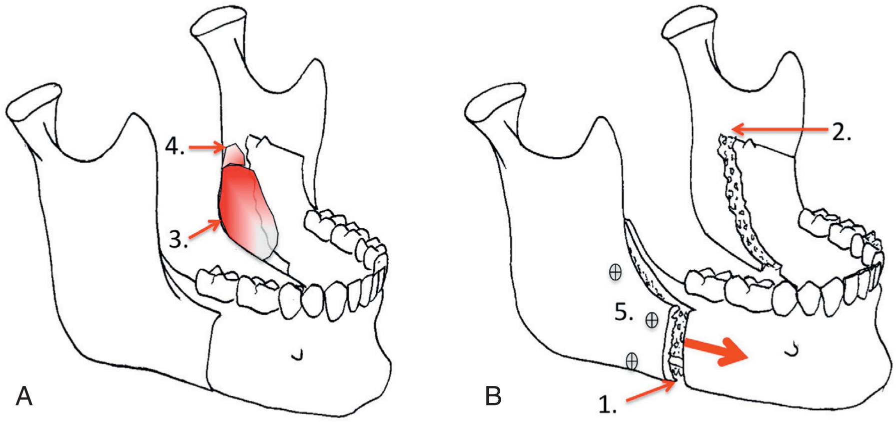

Fig. 21.18 (A, B) The surgical design of the bilateral sagittal split ramus osteotomy for mandibular advancement procedure (*arrow*). A few important technical points are as follows: (1) The vertical corpus osteotomy should include the lower border of the mandible; and (2) the horizontal osteotomy on the medial side of the ramus should be carried just past the lingula into the fossa, superior to the inferior alveolar foramen. The author believes that it is advantageous to strip the medial pterygoid muscle (3) and stylomandibular ligament (4) attachments from the mandibular angles. It allow for more accurate condylar positioning and control of the proximal segment. The segments are rigidly fixated by means of three bicortical positioning screws on each side (5) in this case; however, intersegmental plates and screws may be used.

Fig. 21.19 Case 11. A 9-year-old patient suffering from severe mandibular deficiency. The facial deformity is evident in the frontal (A), profile (B), and three quarter (C) views. A 15-mm surgical advancement by means of distraction osteogenesis planned in (G) and (H). The postdistraction results are demonstrated in (D-F)

Fig. 27.7 The inferior screws are inserted, securing the chin segment to the plate. The segment can now rest against the mandible facilitating superior screw insertion.

Fig. 27.8 The plate is secured, and the chin projection and labiomental crease can now be assessed before final closure.

- Once the chin plate is secured, the incision is loosely approximated, and the patient's face is evaluated from the side to make sure that both the anterior movement and the acuity of the labiomental fold are acceptable to the surgeon.
- If the anterior movement is sufficient but the labiomental fold is too acute, it is possible to position the chin segment inferiorly to soften the acuity of the labiomental fold while preserving the sagittal projection of the chin segment.
- Once the chin has been plated in the proper position, 2-0 Monocryl sutures on an SH needle are used to approximate the mentalis muscle. We usually recommend putting two or three of these in the muscle to restore it to its anatomic position and prevent postoperative chin ptosis. When passing the needle through the mentalis on the skin side, it is important to ensure that the skin is not puckered as the suture is tightened. This can be checked by pulling on the suture after it has been placed (Fig. 27.9). If puckering is noted, redo the suture with a bite less superficial to the skin. Also, the bites should correspond to the labiomental fold to minimize soft tissue distortion from the mentalis closure. Finally, the sutures are held on hemostats until all have been placed to maintain visualization while placing them. After all the sutures are placed, they are tied to approximate the mentalis. After the mentalis is approximated, the mucosa is closed with interrupted 4-0 chromic sutures on a tapered needle.

Fig. 27.9 It is important to verify that the mentalis suture is not too superficial on the skin of labiomental mental crease. Dimpling from the superficial sutures may lead to an unpleasant appearance after surgery.